The Synergy between a Silver-Ruthenium Antimicrobial and aminoglycosides is based on severe macromolecular damage

Emmanuel P. Oladokun[1], Gracious Y. Donkor[1], Julius K. Narh[1], Grady D. Jacobson[1], Cade Ward[1], Patrick O. Tawiah[1], Lisa K. Polzer[1], Kevin A. Edwards[1], Kyle A. Floyd[1], and Jan-Ulrik Dahl[1;*]

[1] School of Biological Sciences, Illinois State University, Normal, IL

Running Title: Reactive oxygen species in antimicrobial therapy

*Address correspondence to Dr. Jan-Ulrik Dahl, School of Biological Sciences, Illinois State University, Campus Box 4120, Normal, IL 61790, phone: (309) 438-7694, email: jdahl1@ilstu.edu

ABSTRACT

The rise of multidrug-resistant (MDR) bacterial pathogens, including uropathogenic *Escherichia coli* (UPEC), highlights the urgent need for alternative treatment strategies to restore antibiotic efficacy. The silver-ruthenium antimicrobial AGXX® exerts potent bactericidal effects through the production of reactive oxygen species (ROS); however, its potential synergy with antibiotics has not been thoroughly investigated. Here, we show that sublethal concentrations of AGXX® strongly enhance aminoglycoside-mediated killing across a diverse panel of Gram-negative and Gram-positive MDR clinical isolates, including highly aminoglycoside-resistant strains. Combinational treatments significantly reduced the effective concentrations of gentamicin, tobramycin, kanamycin, and amikacin required for bacterial killing. Mechanistic analyses revealed that AGXX®/aminoglycoside co-treatment induces pronounced intracellular ROS accumulation, resulting in severe proteotoxic stress, extensive protein aggregation, and DNA damage. Scavenging ROS abolished synergistic killing, establishing oxidative imbalance as the primary driver of the synergy between both antimicrobials. We further identify polyphosphate as a key bacterial defense mechanism that mitigates ROS accumulation, proteotoxicity, and genotoxic stress during combinational treatment. Moreover, AGXX®–aminoglycoside synergy was preserved in an artificial urine medium and across clinical UPEC isolates, underscoring its relevance to urinary tract infections. Together, these findings position AGXX® as a potent aminoglycoside adjuvant that restores antibiotic efficacy through ROS-driven macromolecular damage, supporting its development for combination therapies against MDR bacterial infections.

INTRODUCTION

Originally isolated from *Streptomyces spp.* and *Micromonaspora*, respectively, aminoglycoside antibiotics have now also been developed as semisynthetic derivatives (1). These bactericidal antimicrobials are polycationic and enter bacteria in three steps. Firstly, establishing ionic interactions between the polycationic moieties of aminoglycosides and negatively charged components of the cell surface, including those found in lipopolysaccharide (LPS) (2, 3) displaces divalent cations from aminoglycoside binding sites. This, in turn, results in the destabilization of LPS components and the disruption of outer membrane integrity in an energy-independent way (4). Driven by an increased proton motive force, particularly in aerobically respiring bacteria,

46 aminoglycosides cross the plasma membrane and enter the cytoplasm, where they bind to the
47 aminoacyl-tRNA recognition site and interact with the 16S ribosomal RNA, ultimately causing
48 protein mistranslation that can lead to protein misfolding [recently reviewed in (1)]. Misfolded
49 proteins can be inserted into the plasma membrane and form irregular membrane channels that
50 further exacerbate aminoglycoside uptake and subsequent bactericidal effects (5, 6). Although
51 controversial (7), ROS production resulting from hyperactivation of the electron transport chain in
52 aerobically respiring bacteria has been proposed as a potential contributor to the bactericidal
53 activity of aminoglycosides (5, 6, 8). Likewise, aminoglycoside resistance observed in most
54 anaerobic bacteria could be explained by a lack of sufficiently high proton motive force that
55 aminoglycoside uptake depends on (5, 9). Moreover, Ezraty *et al.* showed that iron-sulfur cluster-
56 containing proteins play an important role in aminoglycoside uptake, ultimately contributing to the
57 bactericidal effects of these antibiotics (10).
58
59 Resistance to aminoglycosides has now been reported in all ESKAPEE pathogens, including the
60 Gram-negative bacterium *Escherichia coli*. *E. coli* colonizes the gastrointestinal (GI) tract of
61 human newborns shortly after birth, where they establish themselves as part of the commensal gut
62 microbiome. Beyond commensal symbiosis, additional *E. coli* serotypes can be pathogenic,
63 resulting in life-threatening diarrheal disease, including enteropathogenic, enterohemorrhagic,
64 enterotoxigenic, enteroinvasive, enteroaggregative, and diffusely adherent *E. coli* serotypes (11).
65 Moreover, extraintestinal pathogenic *E. coli* serotypes (ExPEC) can often still colonize the GI tract
66 and serve commensal functions. It is only after dissemination from the GI tract and entry into their
67 primary site of infection that ExPEC strains become pathogenic. The most common ExPEC
68 serotype is uropathogenic *E. coli* (UPEC), the etiologic agent of most urinary tract infections
69 (UTIs) (11). UPEC traverse the urethra to establish infection within the bladder (cystitis) and can
70 further ascend the ureters to cause infection within the kidneys (pyelonephritis), which, if left
71 untreated, can result in the development of potentially life-threatening septicemia (12, 13). UTIs
72 account for approximately 20% – 50% of all nosocomial infections (14), many of which occur in
73 catheterized patients. Biofilm formation on in-dwelling urinary catheters is the main driving force
74 behind catheter-associated UTIs (CAUTIs) and serves as a reservoir for continued seeding of
75 infection within the urinary tract (12, 13, 15). There is also increasing evidence of the presence of
76 antimicrobial resistance (AMR)- related genes in UPEC (16). The inherent infection mechanisms

77 of UPEC, the ability to form catheter-associated biofilms, and the rise in prevalence of AMR
78 highlight the urgent need for the development of improved antimicrobial compounds and catheter
79 surface coatings to treat or prevent UTI (17, 18).
80
81 Despite its long-standing history and high efficacy against bacteria, the antimicrobial mode of
82 action of silver (Ag) remains poorly understood, although changes in DNA condensation,
83 membrane alteration, and protein damage have been associated with Ag (19). Ag^+ ions interact
84 with cysteine thiols, destabilize iron-sulfur clusters, replace metal-containing cofactors, and and
85 elicit reactive oxygen species (ROS) generation, thereby damaging a wide range of proteins (19).
86 Over the last two decades, silver derivatives have received increased attention for use as
87 antimicrobial surface coatings that can protect from biofilm-forming bacteria and reduce the risk
88 of nosocomial infections (20). One such silver-containing surface coating is AGXX® (21, 22). All
89 AGXX® formulations consist of a silver-ruthenium complex, but differ in the silver-ruthenium
90 ratio, particle size, and production procedure, which may affect their antimicrobial activity (23,
91 24). AGXX® has been shown to be more potent than silver alone, inhibiting the growth of a range
92 of pathogenic bacteria by eliciting a thiol-specific oxidative stress response (22, 25–27). We
93 recently reported that AGXX® potentiates the efficacy of aminoglycoside antibiotics, when used
94 in combination, against the opportunistic pathogen *Pseudomonas aeruginosa* (26). The synergistic
95 bactericidal effects against *P. aeruginosa* are mediated by elevated ROS levels in the cells, which
96 disrupt Fe/S-clusters in metabolic enzymes, lead to elevated free iron, trigger hydroxyl radical
97 formation, and result in a significant increase in outer and inner membrane permeability to
98 exacerbate aminoglycoside influx into the cell (26).
99 In this study, we provide novel insights into the cellular consequences of the synergy between
100 AGXX® and aminoglycosides across a variety of Gram-positive and Gram-negative pathogens,
101 including UPEC and highly aminoglycoside-resistant clinical isolates of various ESKAPEE
102 pathogens. This synergy appears to primarily rely on the generation of ROS, as co-supplementation
103 with an antioxidant abolishes AGXX®/aminoglycoside-induced cell death. For the first time, we
104 provide direct evidence that AGXX®/aminoglycoside co-treatments promote extensive protein
105 aggregation and induce DNA damage. Despite the potent toxicity of AGXX®/aminoglycoside co-
106 treatment, we found that UPEC can activate sophisticated defenses by expressing molecular
107 chaperones, such as IbpA, and by producing the chemical chaperone polyphosphate (polyP). We

108 observed that polyP reduces intracellular ROS accumulation, thereby decreasing DNA damage
109 and protein aggregation, and positively affects UPEC survival, underscoring the significant role of
110 polyP in oxidative stress defense.
111

112 **RESULTS**

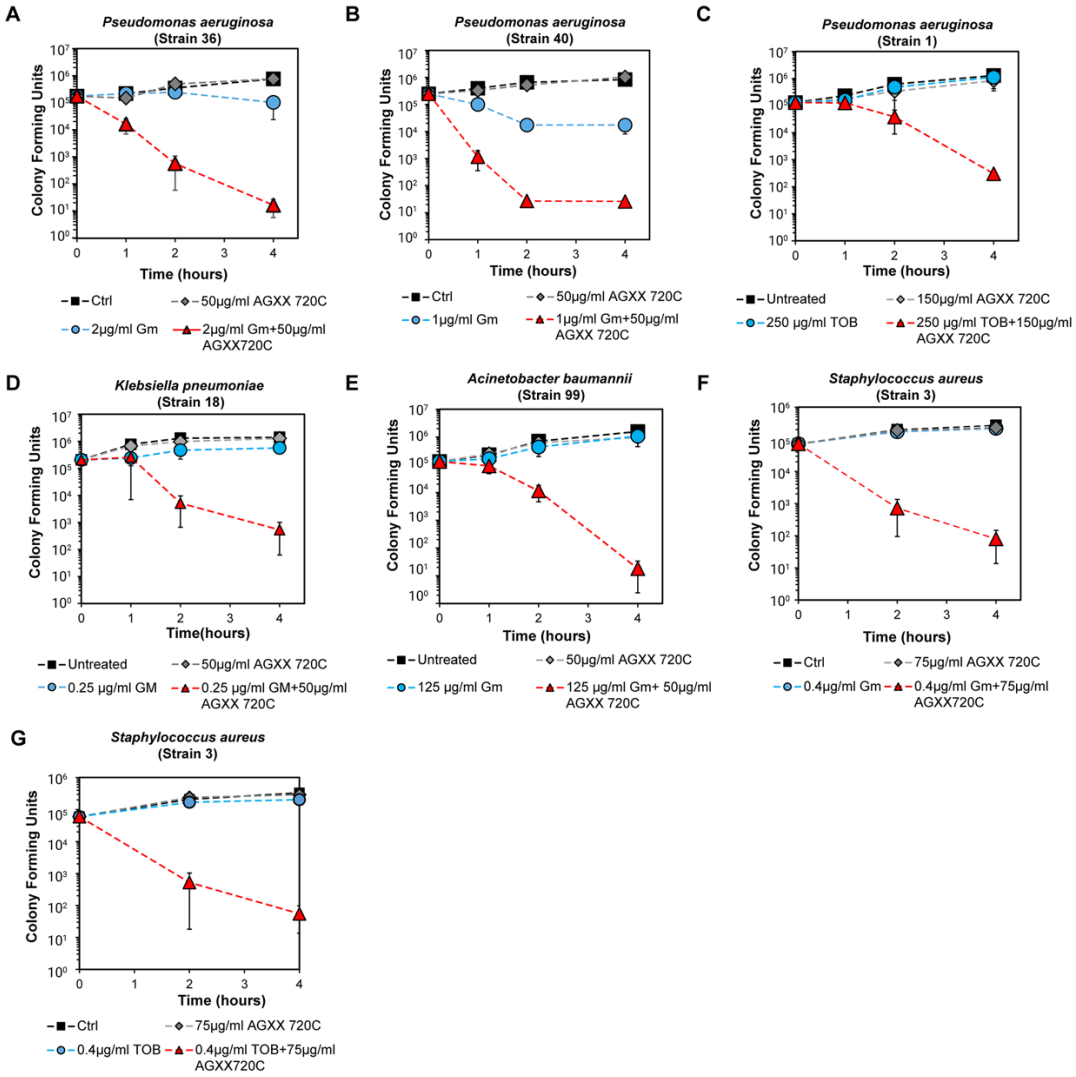

113

114 **Fig. 1. AGXX® enhances the bactericidal effects of aminoglycoside antibiotics in various**
115 **multidrug-resistant ESKAPEE pathogens.** Time-killing survival studies were performed on
116 various clinical isolates of *P. aeruginosa* (**A–C**), *K. pneumoniae* (**D**), *A. baumannii* (**E**), and *S.*
117 *aureus* (**F, G**). Mid-log phase cells were exposed to sublethal concentrations of gentamycin (Gm),
118 tobramycin (TOB), AGXX®720C, or combinations as indicated. Bacterial survival was quantified
119 by determining colony-forming units (CFUs) at the indicated time points post-treatment (0–4 h).
120 (n = 3, ±SD).

121 **AGXX® enhances the bactericidal effects of aminoglycoside antibiotics in various multidrug-**
122 **resistant pathogens.** The rapid emergence of multidrug-resistant pathogens (MDR) requires
123 alternative treatment options, including therapies that enhance the effectiveness of existing
124 antibiotics. The silver-ruthenium antimicrobial AGXX®, which was shown to be effective against
125 laboratory strains of both Gram-positive and Gram-negative pathogens (22–25, 27, 28), may
126 provide such an opportunity. As previously reported by us, AGXX® potentiates the activity of
127 aminoglycoside antibiotics in the laboratory *P. aeruginosa* strain PA14, which is due to elevated
128 aminoglycoside uptake as a result of ROS-induced membrane damage (26). To exclude strain-
129 specific effects and assess the effectiveness of AGXX®/aminoglycoside combinations against
130 other bacterial pathogens, we examined the impact of AGXX®/aminoglycosides against a panel of
131 Gram-negative and Gram-positive clinical isolates obtained from burn-wound patients. With
132 minimal inhibitory concentrations (MIC) between 1 and >2,000 μg/mL, these isolates differ quite
133 significantly in their susceptibility to gentamycin (Gm) and tobramycin (Tob), respectively
134 (**Supplementary Table S1**). We exposed *P. aeruginosa* strains 1, 36, and 40; *Klebsiella*
135 *pneumoniae* strain 18; *Acinetobacter baumannii* strain 99; and *Staphylococcus aureus* strain 3 to
136 the indicated sublethal concentrations of AGXX®720C, aminoglycosides, or their combination and
137 monitored bacterial survival for 4 hours by enumerating colony-forming units (CFUs). Individual
138 treatments with sublethal concentrations of AGXX®720C or aminoglycoside had minimal (*P.*
139 *aeruginosa* strains 36 and 40) to no bactericidal effects across these strains (**Fig. 1A–G**). In
140 contrast, combinational treatments with AGXX®720C and aminoglycosides resulted in rapid
141 synergistic killing, with ~3-log or greater reductions in CFUs observed in all tested strains after 4
142 hours. This effect was particularly pronounced against *P. aeruginosa* strain 1 and *A. baumannii*
143 strain 99, which both have Gm/Tob MICs >500 μg/mL (**Supplementary Table S1**). Notably, sub-
144 MIC concentrations of Gm/Tob, combined with AGXX®720C, significantly reduced survival by
145 more than 3-log, thereby rendering these highly resistant isolates sensitive to aminoglycosides
146 again (**Fig. 1C, 1E**). These findings demonstrate the therapeutic promise of AGXX® as a broad-
147 spectrum compound capable of enhancing aminoglycoside activity against both Gram-negative
148 and Gram-positive MDR pathogens.

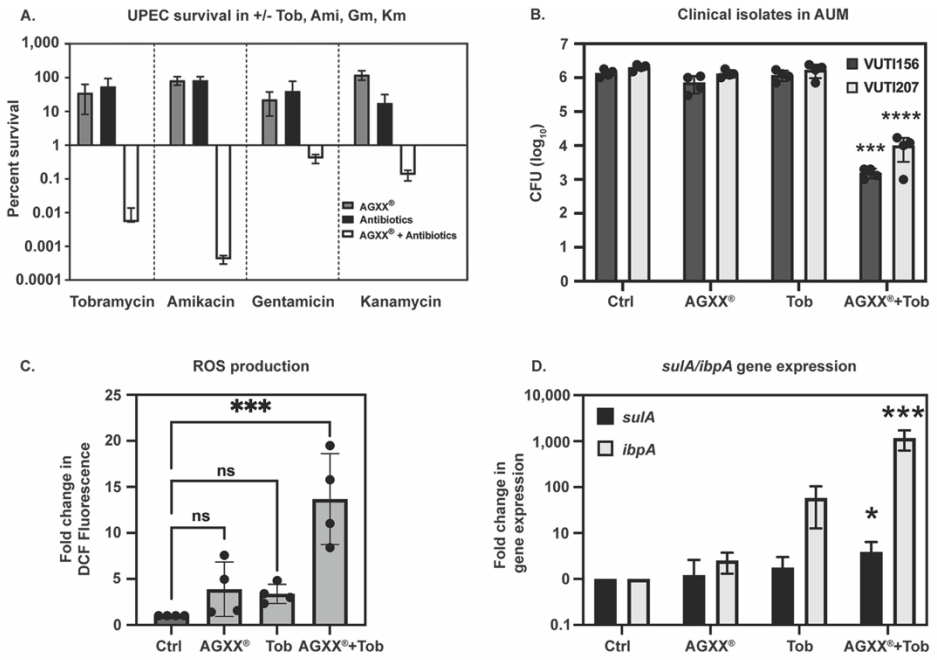

Fig. 2. AGXX®/aminoglycoside co-treatment causes severe oxidative stress and elicits stress responses in UPEC. (A) Exponentially growing cells of the UPEC strain CFT073 were exposed to sublethal concentrations of tobramycin (Tob, 0.75 µg/mL), amikacin (Ami, 0.875 µg/mL), gentamicin (Gm, 0.01 µg/mL), kanamycin (Kan, 1 µg/mL), or AGXX®394C (30 µg/mL), individually and in combination. CFU counts were determined after 3 hours of incubation. The % survival, normalized to untreated CFUs, is plotted (n = 3-4, ±SD). **(B)** UPEC clinical isolates VUTI207 and VUTI156 were grown in artificial urine media (AUM) and treated with 1 µg/mL Tob or 30 µg/mL AGXX®394C individually and in combination. CFU counts were determined after 1 hour of incubation (n = 4, ±SD; statistical analysis: One-way ANOVA, Šídák's multiple comparison test [compared to untreated controls], *** $P < 0.001$, **** $P < 0.0001$). (**C-D**) Mid-log phase CFT073 cells were treated with sublethal concentrations of Tob (0.5 µg/mL) or AGXX®394C (30 µg/mL) individually and in combination. **(C)** ROS levels were measured by H2DCFDA fluorescence (n = 4, ±SD, statistical analysis: One-way ANOVA, Dunnett's posttest, ns = $P > 0.05$, *** $P < 0.001$). (**D**) *ibpA* and *sulA* transcript levels were determined by qRT-PCR. Expression of each gene was normalized to the housekeeping gene *rrsD* and calculated as fold change relative to untreated cells (n = 4, ±SD; statistical analysis: One-way ANOVA, Šídák's multiple comparison test [compared to untreated controls], * $P < 0.05$, *** $P < 0.001$).

AGXX®/aminoglycoside co-treatment causes severe oxidative stress in uropathogenic *E. coli* (UPEC). Silver and silver-containing compounds have become increasingly popular as surface coatings on medical devices, such as catheters, to prevent bacterial attachment and reduce the risk of developing CAUTIs, a significant health problem for hospitalized patients and those living in long-term care facilities (15). The most prominent causative agent of CAUTIs is UPEC, which readily adheres to catheters and forms stress-/treatment-resistant biofilms. To examine the efficacy of AGXX®/aminoglycoside combinational treatment of UPEC, we treated mid-log phase CFT073

175 cells with sublethal concentrations of Tob, amikacin (Ami), Gm, or kanamycin (Kan), alone and
176 in combination with 30 µg/mL of a more recent AGXX® formulation (*i.e.,* AGXX®394C), and
177 quantified bacterial survival via CFU enumeration after 180 minutes. Individual treatments of
178 AGXX®394C and the four aminoglycosides had minimal effects on CFT073, only reducing
179 survival by less than 1-log (**Fig. 2A**). However, combination treatment of AGXX®394C and any
180 aminoglycoside (most notably Tob and Ami), decreased CFT073 survival by up to 4-logs (**Fig.**
181 **2A**). A similar synergistic effect was observed for AGXX®394C/Tob treatment of two UPEC
182 clinical isolates VUTI156 (pyelonephritis) and VUTI207 (cystitis) after 60 minutes, which further
183 demonstrates combinatorial effects with clinically relevant UPEC isolates (**Fig. 2B**). These
184 experiments were conducted in artificial urine media (AUM), to more closely mimic conditions
185 found within the urinary tract (29). Next, we sought to characterize the strength of the synergistic
186 interaction between AGXX® and aminoglycosides in CFT073. We performed a checkerboard
187 assay at varying concentrations of Gm, Kan, Ami, and Tob, with or without 30 µg/mL
188 AGXX®720C. We observed that the addition of AGXX®720C reduced the aminoglycoside
189 concentrations required for complete growth inhibition by 16.7-fold for Gm, 3-fold for Kan, 4-
190 fold for Ami, and 3.8-fold for Tob (**Supplementary Figure S1**), indicating that AGXX®
191 potentiates aminoglycoside antibiotics, independent of the type of aminoglycoside and/or AGXX®
192 formulation used.
193
194 In *P. aeruginosa*, we previously showed that the synergistic effect between AGXX® and sub-lethal
195 aminoglycoside concentrations is attributed to increased accumulation of ROS (26). We observed
196 a similar ROS accumulation in UPEC strain CFT073, where neither AGXX®394C nor Tob alone
197 increased ROS levels, but AGXX®394C co-treatment with a sub-lethal Tob concentration resulted
198 in a ~13-fold increase in ROS levels relative to untreated controls (**Fig. 2C**). Increased ROS levels
199 pose a risk to cellular macromolecules, especially proteins and nucleic acids (30, 31). However,
200 bacteria have evolved intricate systems to deal with the negative consequences of ROS and
201 eliminate ROS-mediated damage, including through transcriptional upregulation of heat-shock
202 and SOS responses (32–36). To determine if AGXX®394C/Tob co-treatment elicits increased
203 responses indicative of macromolecular damage, we examined the transcript levels of hallmark
204 genes for protein aggregation (*i.e., ibpA*) and DNA damage (*i.e., sulA*) using qRT-PCR. Expression
205 of *ibpA*, encoding a small heat shock protein that protects against proteotoxic stress (37), was

206 induced 2.5-fold and 58-fold by individual exposure to AGXX®394C or Tob, respectively, while
207 no significant change in expression of the gene *sulA*, a gene encoding for the SOS cell division
208 inhibitor activated during DNA damage (38), was observed with individual treatments (**Fig. 2D**).
209 However, AGXX®394C/Tob co-treatment resulted in over 1,000-fold increase in *ibpA* and a 5-
210 fold increase in *sulA* expression (**Fig. 2D**), suggesting that the synergy between AGXX® and
211 aminoglycosides in CFT073 may be based on a more pronounced macromolecular damage.

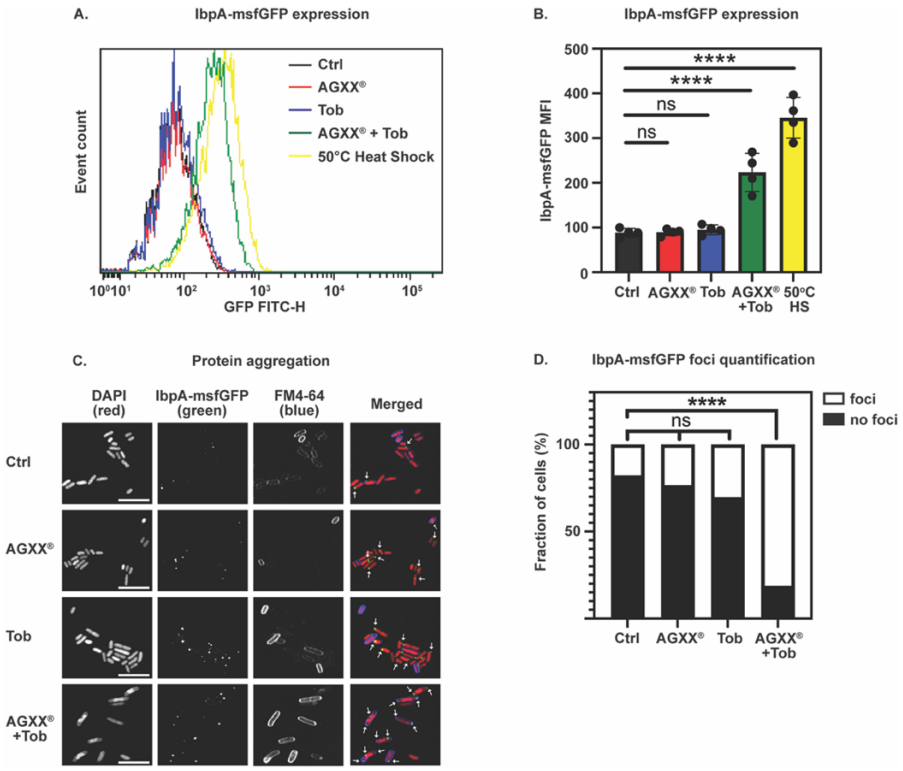

212

213 **Fig. 3. The synergy between AGXX® and aminoglycosides is due to increased proteotoxic**
214 **effects, evoking elevated expression of molecular chaperones**. Cellular IbpA-msfGFP
215 fluorescence was quantified after 1 hour of exposure of mid-log phase *E. coli* cells to sublethal
216 concentrations of AGXX®394C (15 µg/mL), Tob (0.3 µg/mL), or their combination. Untreated
217 cells serve as the negative control, and 50°C heat-shocked cells as the positive control. (**A**) Total
218 cellular IbpA-msfGFP fluorescence determined by flow cytometry. One representative dataset of
219 four biological replicates is shown (scale bar: 7.5 µm). (**B**) Quantification of mean fluorescence
220 intensity (MFI) of IbpA-msfGFP fluorescence determined by flow cytometry (n = 4, ±SD;
221 statistics: One-way ANOVA, Dunnett's multiple comparison test, ns = $P > 0.05$, ****$P < 0.0001$).
222 (**C**) For visualization and quantification of protein aggregates *in vivo*, cells were stained with DAPI
223 (to visualize nucleic acids, red) and FM4-64 (to visualize membranes, blue). White arrows indicate
224 foci formed by IbpA-msfGFP (green) binding to protein aggregates *in vivo*. Images representative
225 of three biological replicates. (**D**) Quantification of the number of foci per cell from microscopy
226 images as shown in **(C)** (n=3, statistics: Two-way Annova, Tukey's multiple comparison test, ns
227 = $P > 0.05$, ****$P < 0.0001$).

228 **The synergy between AGXX® and aminoglycosides is due to increased proteotoxic effects,**
229 **evoking elevated expression of molecular chaperones.** Following up on our transcriptional data
230 pointing towards increased macromolecular damage in bacteria treated with AGXX®394C/Tob
231 combinations, we assessed the extent of protein aggregate formation *in vivo* in the presence and
232 absence of individual or combined treatments with sublethal AGXX®394C and/or Tob
233 concentrations. We utilized a reporter strain harboring a chromosomal fusion between *ibpA* and
234 monomeric superfolder green fluorescent protein under the control of the native *ibpA* promoter.
235 IbpA expression is induced under stress conditions that induce protein unfolding (39), and IbpA-
236 msfGFP has been used previously to monitor and quantify protein aggregation *in vivo* (27, 40).
237 We exposed *E. coli* cells expressing IbpA-msfGFP to sublethal concentrations of AGXX®394C
238 (15 µg/mL), Tob (0.3 µg/mL), or their combination for 1 hour, and then measured IbpA-msfGFP
239 fluorescence by flow cytometry. As a positive control, we induced protein aggregation via heat
240 shock by exposing cells to 50°C for 60 min, which resulted in the most pronounced IbpA-msfGFP
241 fluorescence (**Supplementary Fig. S2**). The combination treatment of AGXX®394C and Tob
242 induced a substantial shift in fluorescence intensity representing a ~2-fold increase in IbpA-
243 msfGFP fluorescence **(Fig. 3A-B)**, comparable to the 50°C heat-shock control, while there was no
244 significant change in IbpA-msfGFP fluorescence observed for the individual treatments and
245 untreated controls **(Fig. 3A-B)**. Visualization of IbpA-msfGFP fluorescent foci by confocal
246 microscopy showed a similar trend for cells exposed to either individual or combined treatments
247 for 60 minutes (**Fig. 3C-D**). Approximately 25% and 30% of cells showed a single IbpA-msfGFP
248 focus per cell upon individual treatment with AGXX®394C or Tob, respectively, which is
249 comparable to the 20% of cells with a foci observed in untreated cells (**Fig. 3C-D**). However,
250 IbpA-msfGFP foci formation was significantly higher upon AGXX®394C/Tob combinational
251 treatment, where 85% of cells had foci, and approximately 30% of those cells harbored multiple
252 foci per cell (**Fig. 3C-D**). Overall, our results provide direct evidence for increased proteotoxicity
253 as a result of the synergy between AGXX®394C and Tob.

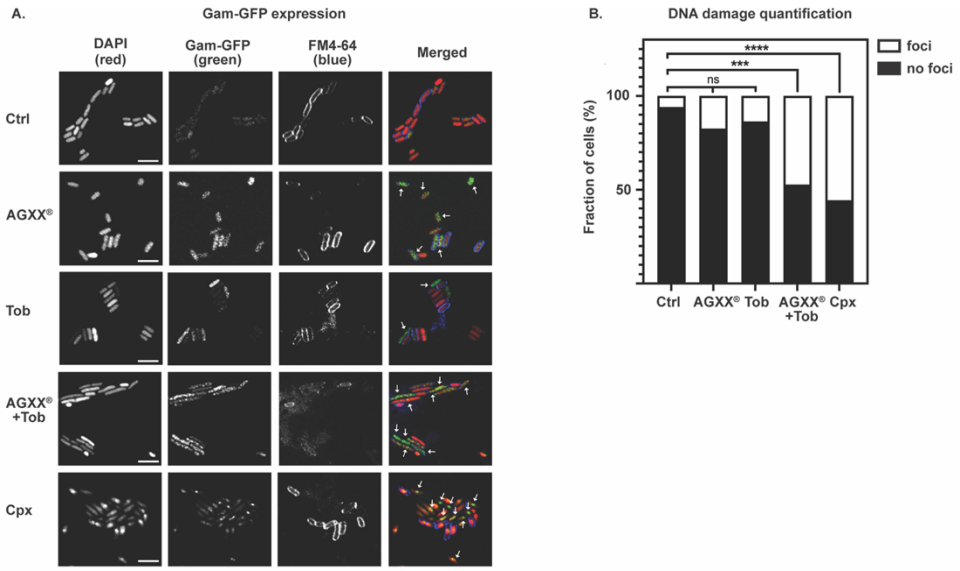

Fig. 4. The AGXX® and aminoglycoside synergy exacerbates DNA damage. (**A, B**) Exponentially growing *E. coli* cells expressing Gam-GFP were treated with sub-lethal concentrations of AGXX®394C (15 µg/mL), Tob (0.3 µg/mL), or a combination thereof for 3 hours. Untreated cells and treatment with 20 µg/mL ciprofloxacin (Cpx) served as controls. Samples were stained with DAPI (red) and FM4-64 (blue). Confocal images were analyzed by blind-counting Gam-GFP (green) foci. (**A**) Arrows indicate Gam-GFP foci representing sites of DNA damage. Images representative of three biological replicates (scale bar: 5 µm). (**B**) Quantification of the number of foci per cell from microscopy images as shown in **(A)** (n=3; statistics: Two-way ANOVA, Tukey's multiple comparison test, ns = $P > 0.05$, ***$P < 0.001$, ****$P < 0.0001$).

The AGXX® and aminoglycoside synergy exacerbates DNA damage. While our qRT-PCR analysis revealed the transcriptional upregulation of *sulA* in response to AGXX®394C/Tob co-treatment (**Fig. 2D**), we next sought to further determine if co-treatment induces significant DNA damage. To monitor and quantify DNA damage, we used *E. coli* cells that overexpress the bacteriophage protein Gam fused to GFP. Gam-GFP has been previously shown to specifically bind to DNA double-strand breaks in both bacterial and mammalian cells (41). Gam-GFP expression was induced by addition of doxycycline in cells either left untreated or treated with AGXX®394C and Tob individually or in combination. Only ~15% and ~18% of cells treated with Tob and AGXX®394C showed one detectable Gam-GFP foci respectively, which did not differ significantly from the ~5% observed in untreated cells (**Fig. 4A-B**). Combinational AGXX®394C/Tob treatment induced a significant increase in Gam-GFP foci, with ~50% of cells having at least one foci, which was comparable to the positive control treatment with ciprofloxacin, a DNA-damaging fluoroquinolone (**Fig. 4A-B**).

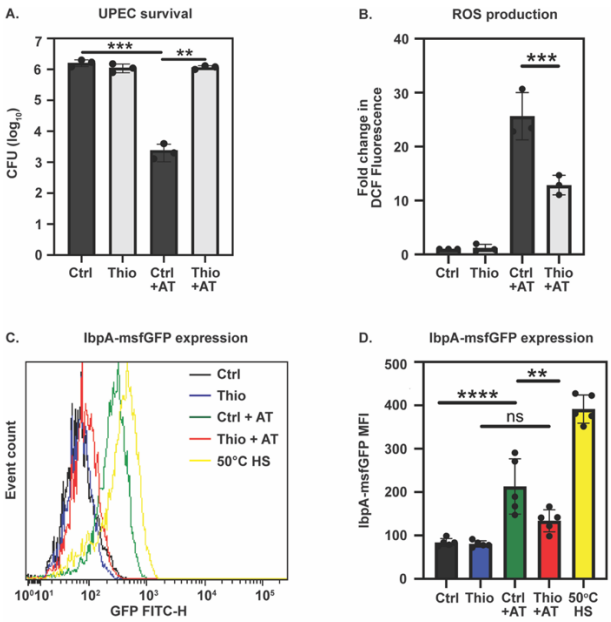

Fig. 5. The ROS-mediated synergistic effects between AGXX® and Tob can be suppressed by antioxidants. (**A, B**) Exponentially growing CFT073 cells were exposed for 60 minutes to a combination of AGXX®394C (30 µg/mL) and Tob (0.5 µg/mL), labelled as "AT". Cells left untreated served as the control. Prior to reaching mid-log phase, cells were either left untreated or pretreated with 70 mM thiourea before subsequent exposure to the combined treatment. (**A**) Bacterial survival was assessed by determining CFUs after 1 hour of treatment. (n = 3, ±SD; statistics: One-way ANOVA, Šídák's multiple comparison test, ** $P < 0.01$, *** $P < 0.001$). (**B**) Intracellular ROS levels were quantified using H2DCFDA fluorescence. (n = 3, ±SD; statistics: One-way ANOVA, Šídák's multiple comparison test, *** $P < 0.001$). (**C, D**) For IbpA-msfGFP expression analysis via flow cytometry, mid-log phase cells were exposed for 60 minutes to either a combination of AGXX®394C (15 µg/mL) and Tob (0.3 µg/mL) (AT), left untreated, or subjected to a heat-shock at 50°C as a positive control. (**C**) Total cellular IbpA-msfGFP fluorescence determined by flow cytometry. One representative dataset of four biological replicates is shown. (**D**) Quantification of mean fluorescence intensity (MFI) of IbpA-msfGFP fluorescence determined by flow cytometry (n = 4, ±SD; statistics: One-way ANOVA, Šídák's multiple comparison test, ns = $P > 0.05$, ** $P < 0.01$, **** $P < 0.0001$).

The ROS-mediated effects generated by AGXX® and Tob synergy can be suppressed by antioxidants. Our data suggest that the increased sensitivity of UPEC to the synergy between AGXX® and aminoglycosides results from augmented intracellular ROS accumulation, which promotes protein aggregation and DNA damage. It has previously been proposed that the bactericidal effects of aminoglycoside antibiotics are at least in part due to the induction of protein misfolding and insertion of misfolded proteins into the plasma membrane to create membrane channels and uncontrolled drug uptake (6, 42). To this end, we examined whether the known ROS scavenger, thiourea, mitigates the cellular stress induced by AGXX®/aminoglycoside combined

305 treatment. To test this, CFT073 cultures were pretreated with thiourea (or left untreated) before
306 exposure to AGXX®394C/Tob co-treatment, and bacterial survival and intracellular ROS levels
307 were determined. As expected, in the absence of thiourea, cells subjected to the combined
308 treatment exhibited a ~3-log reduction in survival (**Fig. 5A**) and a ~25-fold increase in ROS
309 production (**Fig. 5B**). Thiourea pretreatment restored bacterial survival almost completely, and
310 significantly reduced ROS levels by ~50% (**Fig. 5A-B**). Furthermore, pretreatment with thiourea
311 also mitigated the induction of IbpA-msfGFP fluorescence to levels observed under unstressed
312 conditions (**Fig. 5C-D**). These findings further suggest that ROS production is a key contributor
313 to the bactericidal effects of the AGXX®/aminoglycoside combinational treatment.
314

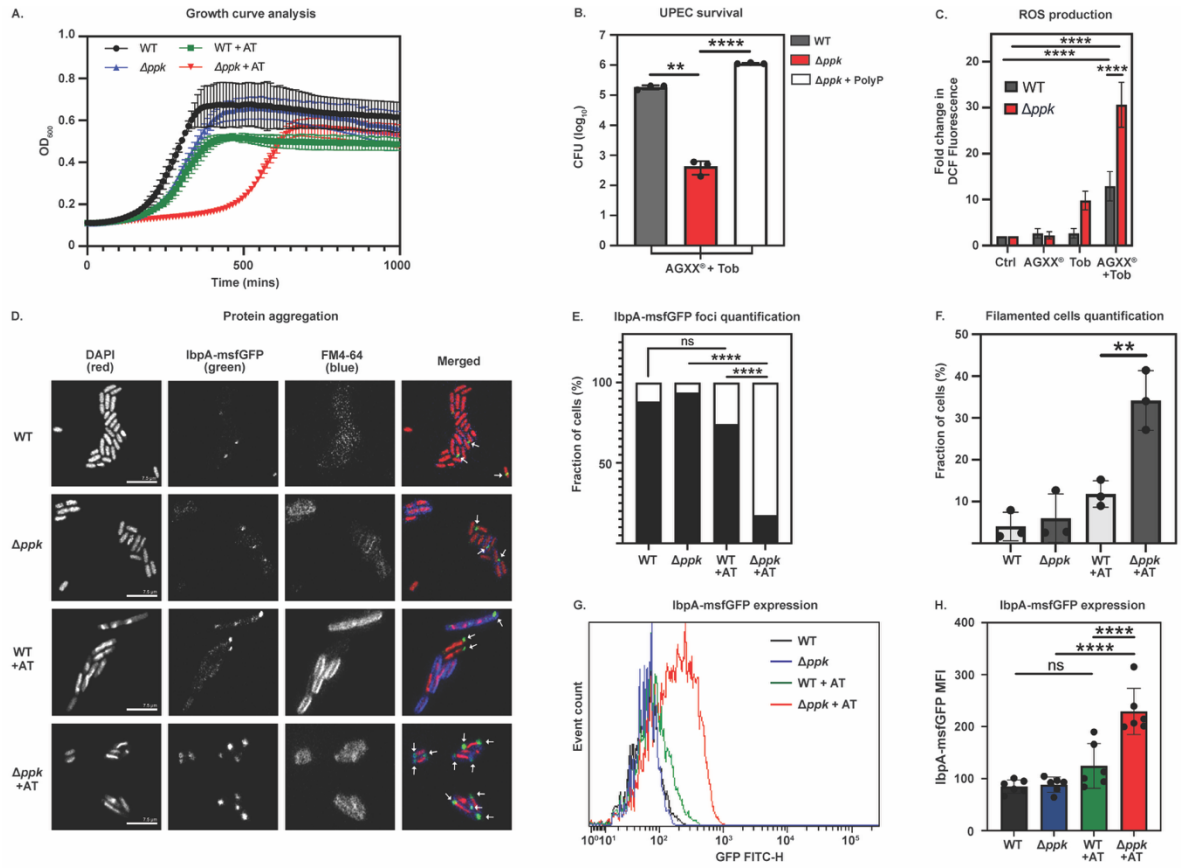

315

316 **Fig. 6. PolyP protects UPEC from AGXX®/aminoglycoside-mediated proteotoxicity.** (**A**)
317 UPEC strains CFT073 and CFT073Δ*ppk* were treated with a combination of AGXX®394C (0.4
318 µg/mL) and Tob (0.2 µg/mL). Growth was monitored over 18 hours. (n = 3, ±SD). (**B, C**) The
319 indicated strains were treated with a combination of AGXX®394C (30 µg/mL) and Tob (0.5
320 µg/mL) for 60 minutes. (**B**) Survival rate as determined by CFU counts (n = 3, ±SD; statistics:
321 One-way ANOVA, Šídák's multiple comparison test, ** P < 0.01, ****P < 0.0001). (**C**)
322 Intracellular ROS levels were quantified using H2DCFDA fluorescence (n = 4, ±SD; statistics:

One-way ANOVA, Šídák's multiple comparison test, **** P < 0.0001). (**D-F**) Exponentially growing WT and Δ*ppk* cells expressing IbpA-msfGFP were left untreated or treated with a combination of AGXX®394C (10 µg/mL) and Tob (0.2 µg/mL) for 1 hour. (**D**) To visualize and quantify protein aggregates *in vivo*, cells were stained with DAPI (red) and FM4-64 (blue). White arrows indicate foci formed by IbpA-msfGFP (green) binding to protein aggregates *in vivo*. Images representative of three biological replicates (scale bar: 7.5 µm). **(E)** Quantification of the number of foci per cell from three biological replicates (n = 3, ±SD; statistics: Two-way ANOVA, Tukey's multiple comparison test, ns = P > 0.05, ****P < 0.0001). **(F**) Quantification of the number of filamentous cells observed in microscopy images as represented in **(D)** (n = 3, ±SD; statistics: One-way ANOVA, Šídák's multiple comparison test, ***P < 0.001). (**G, H**) Total cellular IbpA-msfGFP fluorescence was determined by flow cytometry. (**G**) A representative image from six biological replicates is shown. (**H**) Quantification of mean fluorescence intensity (MFI) of IbpA-msfGFP fluorescence determined by flow cytometry (n = 6, ±SD; statistics: One-way ANOVA, Šídák's multiple comparison test, ns = P > 0.05, **** P < 0.0001).

Polyphosphate protects UPEC from AGXX®/aminoglycoside co-treatment induced proteotoxicity. In addition to activating protein-based molecular chaperones like IbpA, many Gram-negative pathogens can also respond to proteotoxic antimicrobials by converting cellular ATP into polyphosphate (polyP), a chemical chaperone that aids in preventing protein aggregation (43, 44). We recently showed that UPEC cells lacking the enzyme for polyP production (i.e., Δ*ppk*) are more susceptible to AGXX® (27). To test whether polyP protects UPEC from the proteotoxic effects of AGXX®/Tob co-treatment, we analyzed the ability of CFT073 with and without the polyP kinase Ppk1 encoding gene to grow and survive upon exposure to the AGXX®394C/Tob combination. A growth comparison of AGXX®394C/Tob-treated WT and Δ*ppk* cells showed a significantly longer lag phase of polyP-deficient cells (**Fig. 6A**). Notably, when keeping the concentration of one stressor constant while varying the concentration of the other, it became apparent that polyP protects cells from both AGXX®394C and Tob (**Supplementary Fig. S3**). In our survival studies, we exposed exponentially growing WT and Δ*ppk* cells to AGXX®394C/Tob for 1 hour, then serially diluted them for CFU counts. In the absence of Ppk1, AGXX®394C/Tob co-treatment resulted in a ~2.5-log lower survival compared to the wild-type, indicating an increased sensitivity to AGXX®394C/Tob, which could be fully restored by complementation (**Fig. 6B**). Consistent with these findings, we found that Δ*ppk* cells were also characterized by much higher ROS levels upon treatment with Tob alone and when combined with AGXX®394C (**Fig. 6C**). Next, we sought to analyze potential polyP-dependent differences in macromolecular damage using IbpA-msfGFP-expressing WT and Δ*ppk* cells. *E. coli* produces polyP in response to

359 AGXX®394C but not to Tob (**Supplementary Fig. 4A-B**). IbpA-msfGFP-expressing WT and
360 Δ*ppk* cells were exposed to a combination of 10 µg/mL AGXX®394C and 0.2 µg/mL Tob for 1
361 hour, which is a combination of AGXX®394C and Tob concentrations that resulted in the highest
362 IbpA-msfGFP expression in Δ*ppk* (**Supplementary Fig. 4B-D**). Confocal microscopy showed that
363 IbpA-msfGFP foci in untreated WT and Δ*ppk* cells were comparable with 12% and 6% of all cells,
364 respectively (**Fig. 6D-E**). While in WT cells, the combined treatment caused IbpA-msfGFP foci
365 formation in ~20% of the cells; foci were counted in ~85% of Δ*ppk* cells (**Fig. 6D-E**). Activation
366 of the SOS response in bacteria under DNA-damage stress has been shown to block cell division,
367 leading to abnormal growth and filamentation (38, 45). We quantified cell filamentation in
368 AGXX®394C /Tob-treated WT and Δ*ppk* cells, which was ~3-times higher in cells lacking polyP,
369 indicating that DNA damage in polyP-deficient cells is more pronounced (**Fig. 6F**). Flow
370 cytometry analysis further confirmed that AGXX®394C/Tob-induced IbpA-msfGFP expression
371 was much more prominent in polyP-deficient cells (**Fig. 6G-H**). Taken together, our data point
372 towards a critical role for polyP in protecting UPEC from the deleterious effects of
373 AGXX®/aminoglycoside-induced macromolecular damage.
374

375 **DISCUSSION**

376 **AGXX®/aminoglycoside combinations exhibit broad-spectrum antimicrobial activity.** The
377 emergence of antibiotic resistance is an escalating global public health concern. Given the lack of
378 new antimicrobials in the industrial pipeline, novel approaches are desperately needed to combat
379 bacterial pathogens that are otherwise difficult to eradicate. The threat of growing antimicrobial
380 resistance is further compounded by the ability of many pathogenic bacteria to form protected
381 multicellular biofilm communities. Not only does biofilm formation provide defense against
382 antimicrobials, which struggle to diffuse through the extracellular matrix shield, but it also
383 enhances the opportunity for the passage of antimicrobial resistance genes between bacterial
384 species via horizontal gene transfer. Biofilm-mediated resistance, along with antimicrobial
385 resistance, is especially problematic in relation to device-associated nosocomial infections (i.e.,
386 catheter-associated UTIs, intravenous catheter infection, medical implant-associated infections).
387 To combat these ever-evolving threats, a promising area of research has focused on compounds
388 that enhance the efficacy of antibiotics by targeting metabolic processes and/or cellular networks
389 (46). Compounds with synergistic effects have been reported for aminoglycosides (1), as well as

390 beta-lactams (47–49), rifampicin (50), and macrolides (51). Here, we report on the synergistic
391 interaction between aminoglycosides and AGXX®, a ROS-generating surface coating comprised
392 of the two transition metals Ag and Ru. The antimicrobial activity of different AGXX®
393 formulations is attributed to their specific coating composition, including the silver-ruthenium
394 ratio, particle size, and production procedure (27). Silver and silver-containing derivatives such as
395 silver nanoparticles have been previously reported as potent enhancers of aminoglycoside activity
396 in *P. aeruginosa* and other pathogenic bacteria (19, 52–55). These synergies have been shown to
397 have especially meaningful potential clinical implications, with their use as antimicrobial surface
398 coatings on catheters and other medical implants (56). Moreover, silver derivatives such as silver
399 sulfadiazine are currently used in topical applications as a standard for treating and preventing
400 wound infections, despite being associated with side effects such as allergic reactions to the
401 sulfadiazine moiety (57). Intriguingly, AGXX®, which has been shown to be significantly more
402 potent than classical silver and silver sulfadiazine (58), is predicted to cause minimal toxicity to
403 human cells due to minimal release of Ag even after several weeks (25, 28), and, to our knowledge,
404 antimicrobial resistance to AGXX® has not been reported yet. Combined, these characteristics
405 make AGXX® potentially well-suited for applications as a novel antimicrobial surface coating for
406 medical devices.
407
408 Following up on our previous study, showing that AGXX® potentiates the bactericidal activities
409 of aminoglycosides in the Gram-negative opportunistic pathogen *P. aeruginosa* (26), we now
410 provide evidence that the activity of AGXX®/aminoglycoside co-treatments extends to other
411 ESKAPEE pathogens, including MDR-resistant *K. pneumoniae*, *A. baumannii*, *S. aureus*, and
412 UPEC strains (**Fig. 1; Fig. 2A**). Our killing assays revealed that, regardless of the strain tested,
413 exposure to combinatorial AGXX®/aminoglycoside treatment rapidly causes a 3- to 5-log
414 reduction in bacterial survival compared to the individual treatments. Most importantly,
415 AGXX®/aminoglycoside co-treatments reduced the antibiotic concentrations required for efficient
416 killing of clinical ESKAPEE pathogen isolates, which are characterized by high gentamicin and
417 tobramycin resistance, by 8-fold to 16-fold, respectively (**Fig. 1; Supplementary Fig. S1**). This
418 may minimize the risk and/or severity of antibiotic-induced side effects and may also delay or
419 prevent resistance development (59). These data are consistent with our previous observation that

420 AGXX® re-sensitizes an intrinsically resistant *P. aeruginosa* strain to sub-MIC concentrations of
421 kanamycin (26), and underscore the broad-spectrum antimicrobial potential of AGXX®.
422
423 **The synergy between AGXX® and aminoglycosides is based on the induction of severe**
424 **oxidative stress that impairs cellular redox homeostasis.** Our current study further demonstrates
425 that ROS accumulation is the central mechanism underlying the synergistic interaction between
426 AGXX® and aminoglycoside antibiotics. Consistent with our previous observation in *P.*
427 *aeruginosa* (26), fluorescence-based assays in UPEC revealed that AGXX®/aminoglycoside co-
428 treatments induce a ~13-fold increase in intracellular ROS levels compared to individual
429 treatments alone (**Fig. 2**). These elevated ROS levels were tightly linked to the induction of
430 canonical stress response pathways, such as the transcriptional upregulation of *ibpA*, which
431 encodes a small heat-shock protein involved in proteostasis, and *sulA*, a marker of SOS response
432 to DNA damage. Thus, our data point towards significant proteotoxic and genotoxic challenges
433 that AGXX®/aminoglycoside combinations impose on UPEC, likely exceeding the threshold that
434 a functional redox homeostasis can buffer. Flow cytometry and confocal microscopy further
435 demonstrated that AGXX®/Tob co-treatment induced IbpA protein foci to levels comparable to
436 those observed in bacteria under heat shock (Fig. 3). The combinatorial treatment also produced
437 substantial protein aggregation, detected in ~80% of cells. These observations are consistent with
438 established models in which aminoglycosides promote mistranslation and the accumulation of
439 misfolded proteins (10), while AGXX® independently induces oxidative protein damage through
440 thiol oxidation, leading to widespread protein aggregation (22, 27, 60). As a result, expression of
441 molecular chaperones and proteases is highly upregulated in AGXX®-stressed bacteria, as
442 previously shown in several independent transcriptome studies (21–24, 27).
443
444 AGXX® has recently been shown to induce detectable DNA double-strand breaks in a ROS-
445 dependent manner, when applied in sufficiently high yet still sub-lethal concentrations (27). In our
446 present study, AGXX®/Tob co-treated cells exhibited markedly increased DNA damage, as
447 indicated by the formation of Gam-GFP foci (**Fig. 4**). Gam is a bacteriophage protein that binds to
448 sites of double-strand DNA breaks (41). Although aminoglycosides specifically target protein
449 translation, kanamycin has been reported to damage DNA bases, likely via indirect ROS-mediated
450 damage (61). We did not observe significant Gam-GFP foci formation when cells were treated

451 with AGXX® or tobramycin alone, likely due to the low concentrations of each stressor. Strikingly,
452 co-treatment with AGXX®/Tob significantly amplified genotoxic effects, with ~50% of treated
453 cells displaying Gam-GFP foci and ~85% of those cells exhibiting multiple foci. This suggests
454 that the combinatorial treatment with AGXX®/Tob significantly enhances the DNA-damaging
455 ability of AGXX® in UPEC.
456
457 We further demonstrate that ROS are not merely byproducts of, but drivers of,
458 AGXX®/aminoglycoside toxicity. We found that pretreatment with the antioxidant thiourea
459 abolished AGXX®/Tob-induced ROS accumulation, restored bacterial survival to levels
460 comparable to untreated bacteria, and suppressed IbpA protein foci formation and protein
461 aggregation (Fig. 5). These data therefore establish oxidative imbalance as the initiating event
462 linking AGXX® exposure to enhanced aminoglycoside efficacy. This aligns with ROS-dependent
463 models of aminoglycoside killing (5, 26, 62) and reconciles previous controversies (7, 52) by
464 demonstrating that ROS becomes critical when a redox-active compound amplifies
465 aminoglycoside stress. Together, these ROS-driven insults overwhelm bacterial macromolecules,
466 providing a mechanistic explanation for the pronounced bactericidal synergy of AGXX® with
467 aminoglycosides.
468
469 **Bacteria produce polyphosphate to counter AGXX®/aminoglycoside toxicity.** Providing
470 further evidence to support this ROS-driven bactericidal synergy of AGXX® with
471 aminoglycosides, we found that UPEC protect themselves from this toxicity through
472 polyphosphate (polyP) (**Fig. 6, Supplementary Fig. S4**). Gram-negative bacteria have long been
473 known to produce polyP as a stress defense strategy to counter host defense mechanisms (32, 33,
474 63–65). In addition to being involved in various biological processes, including biofilm formation
475 (66, 67), motility (68), virulence factor production (69, 70), and host colonization (66, 69, 71),
476 polyP has also been identified as a potent chemical chaperone that protects bacteria from
477 proteotoxic stress (43, 44, 72, 73). Here, we demonstrate a significant increase in polyP production
478 when cells are exposed to AGXX® **(Fig. S4)**. This is consistent with a previous report that showed
479 that Δ*ppk* cells were highly sensitive to silver nitrate and that the transcriptome of AGXX®-treated
480 UPEC cells exhibited signs of silver exposure (27). While the deletion of *ppk1*, the gene
481 responsible for polyP production, has been associated with increased susceptibility of *E. coli* and

482 *P. aeruginosa* towards aminoglycoside and carbapenem antibiotics (74, 75), we did not detect a
483 significant induction in polyP production in Tob-treated cells (**Fig. S4**). Whether the activation of
484 polyP production is in response to AGXX®/aminoglycosides-generated ROS, or potentially to
485 silver ions that are released from the AGXX® formulation remains unclear. We conclude that
486 PolyP, likely induced by ROS accumulation, acts as a chemical chaperone to protect from the
487 proteotoxic effects of AGXX®/Tob, and propose that both IbpA expression and polyP production
488 are important for a stringent defense. This may explain why, compared to Δ*ppk* strains, IbpA-
489 msfGFP expression is substantially reduced and IbpA-msfGFP foci are present in much fewer cells
490 in the polyP-producing WT strain. In the absence of polyP, cells depend primarily on IbpA-
491 mediated chaperone activity to counter AGXX®/Tob-mediated proteotoxic stress. However, this
492 compensatory mechanism is insufficient to prevent widespread damage, and our data highlights
493 the critical role of polyP in protecting bacterial cells from redox-induced proteome disruptions.
494
495 Collectively, our study positions AGXX® as a dual-function antimicrobial that potentiates
496 aminoglycoside effects on Gram-negative pathogens by intensifying ROS-mediated proteotoxic
497 and genotoxic stress. By driving bacterial stress responses beyond recoverable thresholds, AGXX®
498 potentiates the efficacy of aminoglycoside exposure with detrimental effects on bacterial viability.
499 More broadly, our work highlights controlled redox stress as a rational strategy for antibiotic
500 potentiation and provides a mechanistic framework for the development of ROS-based
501 antimicrobial adjuvants.
502

503 **MATERIALS AND METHODS**

504 **Bacterial strains and growth conditions.** All strains, plasmids, and oligonucleotides used in this
505 study are listed in **Supplementary Table 2**. Unless stated otherwise, overnight cultures were
506 grown aerobically in Luria-Bertani (LB) broth (Millipore Sigma) at 37°C with shaking at 300 rpm
507 for 16-20 hours. For subsequent experiments, overnight cultures were diluted into 3-(N-
508 morpholino) propanesulfonic acid minimal medium supplemented with 0.2% glucose, 1.32 mM
509 K_2HPO_4, and 10 μM thiamine (76), or in artificial urine media (AUM) (29), and incubated at 37°C
510 under shaking conditions.
511

512 **Preparation of artificial urine media (AUM).** AUM was prepared as previously described (29).
513 The final concentrations of the components were as follows: 78.5 mM sodium chloride, 9 mM
514 sodium sulfate, 2.2 mM sodium citrate dihydrate, 0.1 mM sodium oxalate, 3.6 mM potassium
515 dihydrogen phosphate, 21.5 mM potassium chloride, 3 g/L tryptic soy broth, 3 mM calcium
516 chloride, 2 mM magnesium chloride, 15 mM ammonium chloride, 6 mM creatinine, and 200 mM
517 urea (pH 6.3). The AUM was freshly prepared every 7 to 10 days.
518
519 **Preparation of AGXX® formulations.** All AGXX® formulations used in this study were
520 developed and supplied by Largentec GmbH (Berlin, Germany). AGXX®394C and AGXX®720C
521 microparticles used in this study were made from silver powders on cellulose with a particle size
522 between 1.5 and 2.5 µm (MaTeck, Germany). The silver-ruthenium complex was realized by
523 Largentec proprietary electrochemical deposition processes.
524
525 **Time-killing assay of clinical isolates.** Overnight cultures were diluted ~20-fold into MHB by
526 normalizing cultures to an optical density at 600 nm (OD_{600}) = 0.1 in a six-well sterile cell culture
527 plate. Samples were then treated with sublethal concentrations of AGXX®720C and Gm or Tob
528 individually or in combination. Cell culture plates were incubated at 37°C for four hours at 150
529 rpm under aerobic conditions. Cells were collected at the indicated time points, serially diluted in
530 phosphate-buffered saline (PBS, pH 7.4), plated on LB agar, and incubated at 37°C for 20 hours
531 to quantify surviving colonies.
532
533 **Bacterial survival assays.** Overnight cultures of UPEC strains CFT073 or CFT073Δ*ppk* were
534 diluted 50-fold into the indicated media to an initial OD_{600} ~ 0.08 and incubated until reaching an
535 OD_{600} = 0.3. Cultures were then transferred to sterile 125 mL flasks and exposed to sublethal
536 concentrations of AGXX®, the indicated aminoglycosides, or both. If indicated, cultures were
537 pretreated with 70 mM thiourea for 60 minutes before AGXX® and/or aminoglycoside exposure.
538 After 1 hour, aliquots were serially diluted in PBS, plated on LB agar, and incubated overnight at
539 37°C with shaking to determine colony-forming unit (CFU) counts.
540
541 **Checkerboard Assay.** Checkerboard assays were performed as previously described (77), with
542 slight modifications. 100x stock solutions of the indicated aminoglycoside antibiotics were serially

543 diluted and added to the respective wells of 12-well plates, while the concentration of
544 AGXX®720C was held constant across wells. Exponentially growing UPEC CFT073 cultures in
545 MOPSg minimal media were adjusted to an initial OD_{600} of approximately 0.05 and added to each
546 well. Plates were incubated at 37°C with shaking for 16–18 hours. OD_{600} was subsequently
547 measured to assess bacterial growth.
548
549 **Intracellular ROS quantification.** Intracellular ROS levels were quantified using the redox-
550 sensitive dye 2′,7′-dichlorodihydrofluorescein diacetate (H_2DCFDA) (Thermo Fisher Scientific).
551 Exponentially growing cultures of CFT073 and CFT073Δ*ppk* were left untreated or treated with
552 the indicated concentrations of AGXX®394C, Tob, or their combination for 1 hour. Duplicate
553 samples were then collected, washed once with pre-warmed PBS, normalized to an OD_{600} ~1.0 in
554 prewarmed PBS containing 10 µM H2DCFDA, incubated in the dark at 37°C for 30 minutes,
555 rewashed with PBS before DCF fluorescence was measured at excitation/emission wavelengths of
556 485/535 nm in a Tecan Infinite 200 plate reader. If indicated, cells were incubated with 70 mM
557 thiourea, a ROS quencher, prior to stress treatments.
558
559 **Gene expression analysis by qRT-PCR.** Overnight cultures of CFT073 were diluted into MOPSg
560 medium to an OD_{600} ~ 0.08 and grown to mid-log phase (OD_{600} ~ 0.3). Cultures were either left
561 untreated or treated with 30 µg/mL AGXX®394C, 0.5 µg/mL Tob, or their combination. Following
562 10 mins of incubation, transcription was halted by the addition of ice-cold methanol. Total RNA
563 was extracted from at least three biological replicates using a commercial RNA extraction kit
564 (Macherey-Nagel), residual genomic DNA was removed with the TURBO DNA-free kit (Thermo
565 Scientific), and mRNA was reverse transcribed into cDNA using the PrimeScript cDNA synthesis
566 kit (Takara). qRT-PCRs were performed using manufacturer protocols (Alkali Scientific) with
567 gene-specific primers (e.g., *ibpA, sulA*, and *rrsD*). Gene expression was normalized to *rrsD*, and
568 relative transcript levels were determined using the $2^{-\Delta\Delta CT}$ method (78).
569
570 **IbpA-msfGFP expression by flow cytometry.** Overnight cultures of strains MG1655::*ibpA-*
571 *msfGFP* and MG1655Δ*ppk::ibpA-msfGFP* were diluted into fresh MOPSg medium to an OD_{600}
572 ~0.01 and grown to mid-log phase (OD_{600} ~ 0.3). Prior to cultures reaching mid-log phase, cells
573 were then left untreated or pretreated with 70 mM thiourea before the indicated concentrations of

574 AGXX®394C, Tob, or their combination were added for 1 hour. Cells exposed to 50°C for 60 mins
575 served as positive controls. For flow cytometry analysis of IbpA-sfGFP expression, samples were
576 normalized to an OD_{600} of 0.05 in PBS (pH 7.4) and analyzed on a BD FACS Melody cytometer
577 via the FITC channel, recording at least 10,000 events per sample. Data were analyzed with
578 FCSalyzer.
579
580 **IbpA-msfGFP binding to protein aggregates *in vivo*.** Overnight cultures of strains
581 MG1655::*ibpA-msfGFP* and MG1655Δ*ppk::ibpA-msfGFP* were diluted into fresh MOPSg
582 medium to an OD_{600} ~ 0.01 and grown to mid-log phase (OD_{600} ~ 0.3). Prior to cultures reaching
583 mid-log phase, cells were then left untreated or pretreated with 70 mM thiourea before the
584 indicated concentrations of AGXX®394C, Tob, or their combination were added for 1 hour. Cells
585 exposed to 50°C for 60 min served as positive controls. For visualization of IbpA-sfGFP-bound
586 protein aggregates, cells were washed twice in PBS, stained with 5 µg/mL DAPI and 5 µg/mL
587 FM4-64 in the dark for 15 minutes, rewashed, and mounted on 1% agarose pads. Fluorescence
588 microscopy was performed using a Leica SP8 confocal system with a DMi8 CS inverted
589 microscope. At least 500 cells across all replicates were blindly quantified.
590
591 **Gam-GFP binding to DNA double-strand breaks.** Strain MG1655::*gam-gfp* was grown
592 overnight in LB supplemented with 200 ng/mL doxycycline to induce Gam-GFP expression. Cells
593 were diluted into doxycycline-containing MOPSg medium to an OD_{600} ~0.08 and grown to mid-
594 log phase (OD_{600} ~ 0.3), and treated with the indicated concentrations of AGXX®394C, Tob, or
595 their combination. The addition of ciprofloxacin was used as a positive control for DNA damage.
596 Following 3 hours of treatment, cells were washed twice, resuspended in PBS, stained with 5
597 µg/mL DAPI and 5 µg/mL FM4-64 in the dark for 15 minutes, rewashed and resuspended in PBS.
598 Samples were imaged on 1% agarose gel pads using a Leica SP8 confocal system, which is
599 equipped with a DMi8 CS inverted microscope. At least 500 cells across all replicates were
600 counted blindly.
601
602 **Construction of in-frame gene deletions in *E. coli* cells expressing IbpA-msfGFP**. An in-frame
603 *ppk* deletion mutant was constructed using the lambda red-mediated site-specific recombination
604 (79). In brief, the *ppk* gene in *E. coli* MG1655-*ibpA*-msfGFP was replaced by a chloramphenicol

605 resistance cassette, which was subsequently resolved using pCP20 to yield the nonpolar in-frame
606 deleted strain MG1655-*ibpA*-msfGFPΔ*ppk*. The chromosomal mutation was verified by PCR.
607
608 **PolyP extraction and quantification.** Intracellular polyP levels were extracted as previously
609 described (70, 80), with minor modifications, and quantified using DAPI. Mid-log-phase cultures
610 of the IbpA-msfGFP-expressing *E. coli* WT and Δ*ppk*1 strains were grown in MOPSg at 37°C
611 under aerobic conditions and then exposed to the indicated concentrations of Tob or AGXX®394C
612 for 1 h. Following treatment, cultures were normalized to an OD_{600} of 0.3, and 1mL aliquots were
613 harvested by centrifugation at 8,000 x g, 5 min, 4°C. Cell pellets were resuspended in 200 µL
614 guanidinium isothiocyanate (GITC) lysis buffer and incubated at 95°C for 10 min to release
615 intracellular polyP. A 50 µL aliquot of the crude lysate was reserved for total protein determination
616 using the Bradford assay. The remaining lysate was mixed with 95% ethanol and applied to silica
617 membrane EconoSpin columns (Epoch Life Science) for polyP purification. Columns were
618 washed twice with 5 mM Tris-HCl (pH 7.5), and polyP was eluted with 50 mM Tris-HCl (pH 8.0).
619 Eluted polyP was mixed with 25 µM DAPI, incubated in the dark for 10 min, and fluorescence
620 was measured at excitation/emission wavelengths of 420/550 nm, which preferentially detects
621 DAPI–polyP complexes. DAPI in the elution buffer was deducted as the buffer control. Further,
622 the background was determined by treating the purified polyP samples with 1 mg Ppx for an hour
623 prior to staining with DAPI. PolyP concentrations were then extrapolated using a sodium polyP
624 standard curve that was prepared in 50mM Tris HCl, pH 8.0.
625
626 **Growth curve-based assays.** Overnight cultures of CFT073 and CFT073Δ*ppk* were diluted ~50-
627 fold into MOPSg media, grown to early stationary phase, diluted again into fresh MOPSg to an
628 OD_{600} = 0.02, and incubated in a Tecan Infinite 200 plate reader with or without the indicated
629 concentrations of AGXX®394C, Tob, or their combination. Absorbance at 600 nm was measured
630 every 10 minutes for 16 hours.
631
632 **Statistical analyses.** All statistical analyses were performed in GraphPad Prism version 8.0.
633
634

ACKNOWLEDGEMENTS

This work was supported by the NIAID grant 1R03AI174033-01A1 (to J.-U. D.). We thank members of the Dahl and Floyd labs for discussion and feedback. The Largentec GmbH team is acknowledged for providing the different AGXX® formulations and for helpful discussions. Susan Rosenberg (Baylor College of Medicine) and Abram Aertsen (KU Leuven) are acknowledged for strains expressing Gam-GFP and IbpA-msfGFP, respectively.

ETHICS STATEMENT

This work did not involve human subjects or vertebrate animals.

AUTHOR CONTRIBUTIONS

Emmanuel P. Oladokun: investigation, visualization, writing first draft; Gracious Y. Donkor: investigation, review and editing; Julius K. Narh: investigation; Grady D. Jacobson: investigation; Cade Ward: investigation; Patrick O. Tawiah: investigation, review and editing; Lisa K. Polzer: investigation; Kevin A. Edwards: methodology, review and editing; Kyle A. Floyd: review and editing; and Jan-Ulrik Dahl: conceptualization, supervision, funding acquisition, writing – review and editing.

DATA AVAILABILITY STATEMENT

Data available on request from the authors.

CONFLICT OF INTEREST

The authors declare no conflict of interest.

COPYRIGHT STATEMENT

No copyright permissions were needed to be taken.

REFERENCES

1. Tawiah PO, Sultana S, Dahl J-U. 2025. Unlocking Enhanced Efficacy of Aminoglycoside Antibiotics Against Pseudomonas aeruginosa. Microb Biotechnol 18:e70174.

2. Saika T, Hasegawa M, Kobayashi I, Nishida M. 1998. [Ionic binding of 3H-gentamicin and short-term bactericidal activity of gentamicin against Pseudomonas aeruginosa isolates differing in lipopolysaccharide structure]. Kansenshogaku Zasshi 72:97–104.

3. Martin NL, Beveridge TJ. 1986. Gentamicin interaction with Pseudomonas aeruginosa cell envelope. Antimicrob Agents Chemother 29:1079–1087.

4. Joshi T, Voo ZX, Graham B, Spiccia L, Martin LL. 2015. Real-time examination of aminoglycoside activity towards bacterial mimetic membranes using Quartz Crystal Microbalance with Dissipation monitoring (QCM-D). Biochim Biophys Acta 1848:385–391.

5. Kohanski MA, Dwyer DJ, Wierzbowski J, Cottarel G, Collins JJ. 2008. Mistranslation of membrane proteins and two-component system activation trigger aminoglycoside-mediated oxidative stress and cell death. Cell 135:679–690.

6. Davis BD, Chen LL, Tai PC. 1986. Misread protein creates membrane channels: an essential step in the bactericidal action of aminoglycosides. Proc Natl Acad Sci U S A 83:6164–6168.

7. Liu Y, Imlay JA. 2013. Cell death from antibiotics without the involvement of reactive oxygen species. Science 339:1210–1213.

8. Dwyer DJ, Belenky PA, Yang JH, MacDonald IC, Martell JD, Takahashi N, Chan CTY, Lobritz MA, Braff D, Schwarz EG, Ye JD, Pati M, Vercruysse M, Ralifo PS, Allison KR, Khalil AS, Ting AY, Walker GC, Collins JJ. 2014. Antibiotics induce redox-related physiological alterations as part of their lethality. Proc Natl Acad Sci U S A 111:E2100-2109.

9. Ramirez MS, Tolmasky ME. 2010. Aminoglycoside modifying enzymes. Drug Resist Updat 13:151–171.

10. Ezraty B, Vergnes A, Banzhaf M, Duverger Y, Huguenot A, Brochado AR, Su S-Y, Espinosa L, Loiseau L, Py B, Typas A, Barras F. 2013. Fe-S Cluster Biosynthesis Controls Uptake of Aminoglycosides in a ROS-Less Death Pathway. Science 340:1583–1587.

11. Kaper JB, Nataro JP, Mobley HLT. 2004. Pathogenic Escherichia coli. Nat Rev Microbiol 2:123–140.

12. Klein RD, Hultgren SJ. 2020. Urinary tract infections: microbial pathogenesis, host-pathogen interactions and new treatment strategies. Nat Rev Microbiol 18:211–226.

13. Flores-Mireles AL, Walker JN, Caparon M, Hultgren SJ. 2015. Urinary tract infections: epidemiology, mechanisms of infection and treatment options. Nat Rev Microbiol 13:269–284.

14. Saleem Z, Godman B, Hassali MA, Hashmi FK, Azhar F, Rehman IU. 2019. Point prevalence surveys of health-care-associated infections: a systematic review. Pathogens and Global Health 113:191–205.

15. Andersen MJ, Flores-Mireles AL. 2020. Urinary Catheter Coating Modifications: The Race against Catheter-Associated Infections. 1. Coatings 10:23.

16. Timm MR, Russell SK, Hultgren SJ. 2024. Urinary tract infections: pathogenesis, host susceptibility and emerging therapeutics. Nat Rev Microbiol 1–15.

17. Lansdown ABG. 2010. A pharmacological and toxicological profile of silver as an antimicrobial agent in medical devices. Adv Pharmacol Sci 2010:910686.

18. Grass G, Rensing C, Solioz M. 2011. Metallic copper as an antimicrobial surface. Appl Environ Microbiol 77:1541–1547.

19. Barras F, Aussel L, Ezraty B. 2018. Silver and Antibiotic, New Facts to an Old Story. Antibiotics 7:79.

20. Nolan LK, Li G, Logue CM. 2015. Origin and Dissemination of Antimicrobial Resistance among Uropathogenic Escherichia coli. Microbiol Spectr 3.

21. Sobisch L-Y, Rogowski KM, Fuchs J, Schmieder W, Vaishampayan A, Oles P, Novikova N, Grohmann E. 2019. Biofilm Forming Antibiotic Resistant Gram-Positive Pathogens Isolated From Surfaces on the International Space Station. Front Microbiol 10:543.

22. Loi VV, Busche T, Preuß T, Kalinowski J, Bernhardt J, Antelmann H. 2018. The AGXX® Antimicrobial Coating Causes a Thiol-Specific Oxidative Stress Response and Protein S-bacillithiolation in Staphylococcus aureus. Front Microbiol 9:3037.

23. Clauss-Lendzian E, Vaishampayan A, de Jong A, Landau U, Meyer C, Kok J, Grohmann E. 2018. Stress response of a clinical Enterococcus faecalis isolate subjected to a novel antimicrobial surface coating. Microbiological Research 207:53–64.

24. Vaishampayan A, de Jong A, Wight DJ, Kok J, Grohmann E. 2018. A Novel Antimicrobial Coating Represses Biofilm and Virulence-Related Genes in Methicillin-Resistant Staphylococcus aureus. Front Microbiol 9:221.

25. Guridi A, Diederich A-K, Aguila-Arcos S, Garcia-Moreno M, Blasi R, Broszat M, Schmieder W, Clauss-Lendzian E, Sakinc-Gueler T, Andrade R, Alkorta I, Meyer C, Landau U, Grohmann E. 2015. New antimicrobial contact catalyst killing antibiotic resistant clinical and waterborne pathogens. Mater Sci Eng C Mater Biol Appl 50:1–11.

26. Donkor GY, Anderson GM, Stadler M, Tawiah PO, Orellano CD, Edwards KA, Dahl J-U. 2023. A novel ruthenium-silver based antimicrobial potentiates aminoglycoside activity against Pseudomonas aeruginosa. mSphere e0019023.

27. Tawiah PO, Gaessler LF, Anderson GM, Oladokun EP, Dahl J-U. 2025. A novel silver-ruthenium-based antimicrobial kills Gram-negative bacteria through oxidative stress-induced macromolecular damage. mSphere 10:e0001725.

28. Linzner N, Antelmann H. 2021. The Antimicrobial Activity of the AGXX® Surface Coating Requires a Small Particle Size to Efficiently Kill Staphylococcus aureus. Front Microbiol 12:731564.

29. Brooks T, Keevil CW. 1997. A simple artificial urine for the growth of urinary pathogens. Letters in Applied Microbiology 24:203–206.

30. Ezraty B, Gennaris A, Barras F, Collet J-F. 2017. Oxidative stress, protein damage and repair in bacteria. Nat Rev Microbiol 15:385–396.

31. Cooke MS, Evans MD, Dizdaroglu M, Lunec J. 2003. Oxidative DNA damage: mechanisms, mutation, and disease. The FASEB Journal 17:1195–1214.

32. Dahl J-U, Gray MJ, Jakob U. 2015. Protein Quality Control under Oxidative Stress Conditions. Journal of Molecular Biology 427:1549–1563.

33. Sultana S, Foti A, Dahl J-U. 2020. Bacterial Defense Systems against the Neutrophilic Oxidant Hypochlorous Acid. Infect Immun 88:e00964-19.

34. Brand C, Newton-Foot M, Grobbelaar M, Whitelaw A. 2025. Antibiotic-induced stress responses in Gram-negative bacteria and their role in antibiotic resistance. J Antimicrob Chemother 80:1165–1184.

35. Sultana S, Dahl J-U. 2023. A Year at the Forefront of Bacterial Defense Systems Against Neutrophilic Oxidants. Biol Open 12:bio059809.

36. Sen A, Imlay JA. 2021. How Microbes Defend Themselves From Incoming Hydrogen Peroxide. Front Immunol 12:667343.

37. Miwa T, Taguchi H. 2025. Revival of the Escherichia coli heat shock response after two decades with a small Hsp in a critical but distinct act. Biol Chem 406:29–33.

38. Mukherjee A, Cao C, Lutkenhaus J. 1998. Inhibition of FtsZ polymerization by SulA, an inhibitor of septation in *Escherichia coli*. Proc Natl Acad Sci USA 95:2885–2890.

39. Ratajczak E, Zietkiewicz S, Liberek K. 2009. Distinct activities of Escherichia coli small heat shock proteins IbpA and IbpB promote efficient protein disaggregation. J Mol Biol 386:178–189.

40. Govers SK, Mortier J, Adam A, Aertsen A. 2018. Protein aggregates encode epigenetic memory of stressful encounters in individual Escherichia coli cells. PLoS Biol 16:e2003853.

41. Shee C, Cox BD, Gu F, Luengas EM, Joshi MC, Chiu L-Y, Magnan D, Halliday JA, Frisch RL, Gibson JL, Nehring RB, Do HG, Hernandez M, Li L, Herman C, Hastings PJ, Bates D, Harris RS, Miller KM, Rosenberg SM. 2013. Engineered proteins detect spontaneous DNA breakage in human and bacterial cells. Elife 2:e01222.

42. Bryan LE, Kwan S. 1983. Roles of ribosomal binding, membrane potential, and electron transport in bacterial uptake of streptomycin and gentamicin. Antimicrobial Agents and Chemotherapy 23:835–845.

43. Groitl B, Dahl J-U, Schroeder JW, Jakob U. 2017. *Pseudomonas aeruginosa* defense systems against microbicidal oxidants: Defense systems against microbicidal oxidants. Molecular Microbiology 106:335–350.

44. Gray MJ, Wholey W-Y, Wagner NO, Cremers CM, Mueller-Schickert A, Hock NT, Krieger AG, Smith EM, Bender RA, Bardwell JCA, Jakob U. 2014. Polyphosphate Is a Primordial Chaperone. Molecular Cell 53:689–699.

45. Kreuzer KN. 2013. DNA Damage Responses in Prokaryotes: Regulating Gene Expression, Modulating Growth Patterns, and Manipulating Replication Forks. Cold Spring Harbor Perspectives in Biology 5:a012674–a012674.

46. Wright GD. 2016. Antibiotic Adjuvants: Rescuing Antibiotics from Resistance. Trends in Microbiology 24:862–871.

47. Bilal H, Bergen PJ, Kim TH, Chung SE, Peleg AY, Oliver A, Nation RL, Landersdorfer CB. 2019. Synergistic Meropenem-Tobramycin Combination Dosage Regimens against Clinical Hypermutable Pseudomonas aeruginosa at Simulated Epithelial Lining Fluid Concentrations in a Dynamic Biofilm Model. Antimicrob Agents Chemother 63:e01293-19.

48. Giamarellou H, Zissis NP, Tagari G, Bouzos J. 1984. In vitro synergistic activities of aminoglycosides and new beta-lactams against multiresistant Pseudomonas aeruginosa. Antimicrob Agents Chemother 25:534–536.

49. Pankuch GA, Lin G, Kubo A, Armstrong ES, Appelbaum PC, Kosowska-Shick K. 2011. Activity of ACHN-490 Tested Alone and in Combination with Other Agents against Pseudomonas aeruginosa. Antimicrobial Agents and Chemotherapy 55:2463–2465.

50. Poole K, Gilmour C, Farha MA, Mullen E, Lau CH-F, Brown ED. 2016. Potentiation of Aminoglycoside Activity in Pseudomonas aeruginosa by Targeting the AmgRS Envelope Stress-Responsive Two-Component System. Antimicrob Agents Chemother 60:3509–3518.

51. Tré-Hardy M, Nagant C, El Manssouri N, Vanderbist F, Traore H, Vaneechoutte M, Dehaye J-P. 2010. Efficacy of the combination of tobramycin and a macrolide in an in vitro

Pseudomonas aeruginosa mature biofilm model. Antimicrob Agents Chemother 54:4409–4415.

52. Herisse M, Duverger Y, Martin-Verstraete I, Barras F, Ezraty B. 2017. Silver potentiates aminoglycoside toxicity by enhancing their uptake. Mol Microbiol 105:115–126.

53. Morones-Ramirez JR, Winkler JA, Spina CS, Collins JJ. 2013. Silver enhances antibiotic activity against gram-negative bacteria. Sci Transl Med 5:190ra81.

54. Dove AS, Dzurny DI, Dees WR, Qin N, Nunez Rodriguez CC, Alt LA, Ellward GL, Best JA, Rudawski NG, Fujii K, Czyż DM. 2022. Silver nanoparticles enhance the efficacy of aminoglycosides against antibiotic-resistant bacteria. Front Microbiol 13:1064095.

55. Habash MB, Goodyear MC, Park AJ, Surette MD, Vis EC, Harris RJ, Khursigara CM. 2017. Potentiation of Tobramycin by Silver Nanoparticles against Pseudomonas aeruginosa Biofilms. Antimicrob Agents Chemother 61:e00415-17.

56. Lansdown ABG. 2010. A pharmacological and toxicological profile of silver as an antimicrobial agent in medical devices. Adv Pharmacol Sci 2010:910686.

57. Fuller FW. 2009. The side effects of silver sulfadiazine. J Burn Care Res 30:464–470.

58. Carr HS, Wlodkowski TJ, Rosenkranz HS. 1973. Silver sulfadiazine: in vitro antibacterial activity. Antimicrob Agents Chemother 4:585–587.

59. Rosenberg CR, Fang X, Allison KR. 2020. Potentiating aminoglycoside antibiotics to reduce their toxic side effects. PLoS One 15:e0237948.

60. Sultana S, Anderson GM, Hoffmann KP, Dahl J-U. 2021. Extraction and Visualization of Protein Aggregates after Treatment of Escherichia coli with a Proteotoxic Stressor. JoVE (Journal of Visualized Experiments) e62628.

61. Kang TM, Yuan J, Nguyen A, Becket E, Yang H, Miller JH. 2012. The Aminoglycoside Antibiotic Kanamycin Damages DNA Bases in Escherichia coli: Caffeine Potentiates the DNA-Damaging Effects of Kanamycin while Suppressing Cell Killing by Ciprofloxacin in Escherichia coli and Bacillus anthracis. Antimicrob Agents Chemother 56:3216–3223.

62. Kohanski MA, Dwyer DJ, Hayete B, Lawrence CA, Collins JJ. 2007. A Common Mechanism of Cellular Death Induced by Bactericidal Antibiotics. Cell 130:797–810.

63. Rao NN, Gómez-García MR, Kornberg A. 2009. Inorganic Polyphosphate: Essential for Growth and Survival. Annu Rev Biochem 78:605–647.

64. Bowlin MQ, Gray MJ. 2021. Inorganic polyphosphate in host and microbe biology. Trends in Microbiology 29:1013–1023.

65. Gray MJ, Jakob U. 2015. Oxidative stress protection by polyphosphate—new roles for an old player. Current Opinion in Microbiology 24:1–6.

66. Rashid MH, Rumbaugh K, Passador L, Davies DG, Hamood AN, Iglewski BH, Kornberg A. 2000. Polyphosphate kinase is essential for biofilm development, quorum sensing, and virulence of Pseudomonas aeruginosa. Proceedings of the National Academy of Sciences 97:9636–9641.

67. Fraley CD, Rashid MH, Lee SSK, Gottschalk R, Harrison J, Wood PJ, Brown MRW, Kornberg A. 2007. A polyphosphate kinase 1 (ppk1) mutant of Pseudomonas aeruginosa exhibits multiple ultrastructural and functional defects. Proc Natl Acad Sci USA 104:3526–3531.

68. Rashid MH, Kornberg A. 2000. Inorganic polyphosphate is needed for swimming, swarming, and twitching motilities of Pseudomonas aeruginosa. Proceedings of the National Academy of Sciences 97:4885–4890.

69. Neville N, Roberge N, Ji X, Stephen P, Lu JL, Jia Z. 2021. A Dual-Specificity Inhibitor Targets Polyphosphate Kinase 1 and 2 Enzymes To Attenuate Virulence of Pseudomonas aeruginosa. mBio 12:e0059221.

70. Shah R, Narh JK, Urlaub M, Jankiewicz O, Johnson C, Livingston B, Dahl J-U. 2024. Pseudomonas aeruginosa kills Staphylococcus aureus in a polyphosphate-dependent manner. mSphere e0068624.

71. Dahl J-U, Gray MJ, Bazopoulou D, Beaufay F, Lempart J, Koenigsknecht MJ, Wang Y, Baker JR, Hasler WL, Young VB, Sun D, Jakob U. 2017. The anti-inflammatory drug mesalamine targets bacterial polyphosphate accumulation. Nat Microbiol 2:16267.

72. Yoo NG, Dogra S, Meinen BA, Tse E, Haefliger J, Southworth DR, Gray MJ, Dahl J-U, Jakob U. 2018. Polyphosphate Stabilizes Protein Unfolding Intermediates as Soluble Amyloid-like Oligomers. Journal of Molecular Biology 430:4195–4208.

73. Cremers CM, Knoefler D, Gates S, Martin N, Dahl J-U, Lempart J, Xie L, Chapman MR, Galvan V, Southworth DR, Jakob U. 2016. Polyphosphate: A Conserved Modifier of Amyloidogenic Processes. Molecular Cell 63:768–780.

74. Chen J, Su L, Wang X, Zhang T, Liu F, Chen H, Tan C. 2016. Polyphosphate Kinase Mediates Antibiotic Tolerance in Extraintestinal Pathogenic Escherichia coli PCN033. Front Microbiol 7.

75. Ortiz-Severín J, Varas M, Bravo-Toncio C, Guiliani N, Chávez FP. 2015. Multiple antibiotic susceptibility of polyphosphate kinase mutants (ppk1 and ppk2) from Pseudomonas aeruginosa PAO1 as revealed by global phenotypic analysis. Biol Res 48:22.

76. Neidhardt FC, Bloch PL, Smith DF. 1974. Culture medium for enterobacteria. J Bacteriol 119:736–747.

77. Canchola J, Donkor GYB, Tawiah PO, Fasawe A, Ayim E, Engelke MF, Dahl J-U. 2024. Alkyl Pyridinol Compounds Exhibit Antimicrobial Effects against Gram-Positive Bacteria. Antibiotics (Basel) 13:897.

78. Pfaffl MW. 2001. A new mathematical model for relative quantification in real-time RT-PCR. Nucleic Acids Res 29:e45.

79. Datsenko KA, Wanner BL. 2000. One-step inactivation of chromosomal genes in Escherichia coli K-12 using PCR products. Proceedings of the National Academy of Sciences 97:6640–6645.

80. Dahl J, Xie L, Jakob U. 2018. Extraction and Quantification of Polyphosphate (polyP) from Gram-negative Bacteria. BIO-PROTOCOL 8.